Journal of Sound and Vibration (2001) **248**(1), 91–103
doi:10.1006/jsvi.2001.3676, available online at http://www.idealibrary.com on IDEAL®

EXPERIMENTAL DETERMINATION OF THE RUBBING LOCATION BY MEANS OF ACOUSTIC EMISSION AND WAVELET TRANSFORM

Q. WANG AND F. CHU

State Key Laboratory of Tribology, Department of Precision Instruments, Tsinghua University, Beijing 100084, *People's Republic of China. E-mail: chufl@pim.tsinghua.edu.cn*

(*Received* 17 *April* 2000, *and in final form* 26 *March* 2001)

A method to pinpoint the rubbing location in a rotor-bearing system is presented. This method is based on the data sampled by acoustic emission (AE) sensors placed at different bearing supports. Usually, the point where rubbing occurs cannot be detected using the method of cross-correlation directly to the data, due to the noise produced during rubbing and the structure resonance of the signal. Through wavelet transform (WT), signals are decomposed into a series of time-domain signals, each of which covers a specific octave frequency band. Then the method of cross-correlation is applied to the decomposed signals to detect the rubbing location. This method is found to be very effective.

1. INTRODUCTION

The requirement of high efficiency and compactness has made the operation clearance of modern rotating machinery become smaller and smaller, which will increase the probability of rubbing between stationary and rotational parts and thus may cause serious malfunctions. Therefore, the fault diagnosis of rubbing is very important for the safe operation of rotating machinery. A comprehensive research has been performed on the vibration of a rub-impact rotor system. Muszynska's literature survey [1] gave a list of previous papers on the rub-related vibration phenomena during rubbing. Beatty [2] proposed a mathematical model for rubbing forces with piecewise linear form of stiffness and discussed some important points for diagnosing this fault. Choy and Podavan [3] analyzed the effects of different system parameters on rubbing forces and transient responses while Chu and Zhang [4] discussed periodic, quasi-periodic and chaotic vibrations of the system. Based on their research, rub is not so difficult to detect, with some dynamic characteristics such as orbital presentation of shaft motion and the existence of strong higher harmonics. But the determination of the rubbing location, however, is rather difficult, and little research work has been done.

Armor and Graham [5] described the form of acoustic emission signals from turbines and discussed the material characterization tests in the light of this data. They "suggested" that AE appeared to be a viable technique for the detection and location of blade rubbing in their paper. Shao and Zhang [6] developed an on-line monitoring instrument with four channels of AE signal and four channels of vibration signal, which could locate the rubbing fault approximately based on the AE signals. The disadvantage of this instrument is that only if the rubbing is in the vicinity of an AE sensor, can the position be detected. Therefore, this method is not desirable if the rotor is very long and/or unsuitable to mount many

0022-460X/01/460091 + 13 $35.00/0

sensors. Oks *et al.* [7] proposed a method to detect the point where rubbing occurred based on the analysis of the non-linear vibration caused by rubbing. A particular feature of the non-linear vibration is that the amplitude of higher harmonics in the response becomes large in the vicinity of the point where rubbing occurs. The point can thus be detected by investigating the distribution of the amplitude of higher harmonics included in the response along the rotor. However, the distribution of the amplitude of higher harmonics is usually non-homogeneous in a practical rotor unit, and if the rubbing is not strong enough to change the original distribution, the method will generally not give a good result.

A simple method to pinpoint the rubbing location is presented in this paper based on the rubbing experiments. Here two useful tools are used, i.e., the acoustic emission (AE) technique mentioned above and the wavelet transform (WT). One of the major advantages of using acoustic emission to detect the condition of the rub-impact is that the frequency range of the acoustic emission signal is much higher than that of the machine vibration and environmental noise. Therefore, a relatively uncontaminated signal can be easily obtained by the use of a high-pass filter [8]. Another distinct advantage of AE technique is the possibility to calculate the spatial source location based on the arrival time difference between a number of sensors. In this way, the use of two sensors allows for a linear source location [9]. But, the situation of the rubbing in the multisupported rotor system is much complex, and the structural resonances of the rotor system also pose another problem. In fact, the rubbing location can seldom be accurately detected with the experimental data. Thus, another tool named wavelet transform is used, which has been used for several years in such areas as seismic technique, image compression, acoustics, and mechanical vibrations [10]. It is shown that, with the help of WT, the detection of the point where rubbing occurs is much more accurate.

2. EXPERIMENTAL SET-UP

The experimental set-up consists of the rotor kit with four supports and four discs, as shown in Figure 1, and a set of data acquisition system including AE sensors. The four bearings are hydrodynamic lubricating bearings with identical inner diameters of 31 mm. The length of the bearing housing in the axial direction is 40 mm. The four identical discs are approximately symmetric along the solid coupling, and the mass of each disc is 2·205 kg. The diameter of the axle is 12 mm.

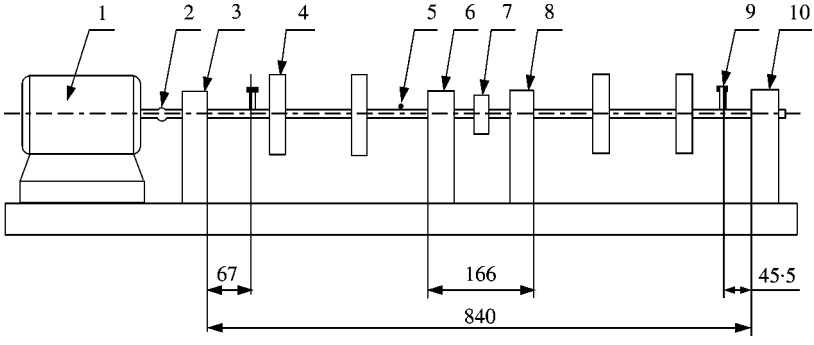

Figure 1. Rotor kit: 1, motor; 2, flexible coupling; 3, first bearing housing; 4, discs; 5, keyphasor; 6, second bearing housing; 7, solid coupling; 8, third bearing housing; 9, rub screw; 10, fourth bearing housing.

The rotor kit was impulse tested to obtain its natural frequencies. The lowest and the second natural frequencies are 56 and 61 Hz respectively. The third and the fourth natural frequencies are 154 and 195 Hz respectively. The rated speed of the 120 W motor is 4000 r.p.m. The rotor is running at a speed of about $4000/60 = 66{\cdot}7$ Hz, between the second and the third natural frequencies.

The material of the rubbing screw is copper and the material of the axle is steel. There are two points where the rubbing screw can be screwed down and fastened, but not simultaneously.

The acoustic emission equipment used for the rubbing diagnosis is named BUAA AE testing system. Three AE probes, two of which are used to pinpoint the rubbing location and the third as a reference, are placed on the side of the bearing housings in the radial direction. The positions of the AE probes are variable. Not only can they be placed on different bearing housings, but they can also be placed on the two sides of the same bearing housing. The band-pass filtered (20 kHz $\sim$ 1·5 MHz) output signal of the sensors was sent to a high-speed 16-bit A/D converter for data sampling at a variable frequency (highest 18181·8 Hz).

3. ACOUSTIC EMISSION TECHNIQUE

Acoustic emission (AE) for the detection of defect growth was pioneered in the late 1940s by Josef Kaiser, who found that engineering materials emitted low-amplitude clicks of sound when they were stressed. In addition to AE sources associated with defect growth (i.e., plastic deformation and crack extension), AE sensors were also found to be sensitive to a plethora of other energy loss mechanisms such as impacts, friction, turbulence, cavitation, spalling, material reduction, etc. [11]. Now, AE technique has become a main-stream non-destructive testing (NDT) method.

Different from vibration signal, the AE signal is converted from sound produced when rubbing occurs. Therefore, it is more related to the condition of the rubbing other than the vibration behaviors of the rotor. If no rubbing between rotor and stator occurs, the sensors usually have no response to such influences as imbalance and misalignment, which are difficult to be removed and will induce higher harmonics in the analysis of vibration signals of a multisupport rotor system. Therefore, AE technique is especially suitable for the multisupport rotor systems, such as steam turbines [12]. But this does not mean that only the AE sensors are enough, because in NDT, one method often cannot provide the whole solution. For cost effectiveness, technical adequacy, or both, it is better to use a combination of different methods [13].

The BUAA AE testing system used in the experiment employs a new feature extraction by the analysis of AE envelope signals, instead of the classical AE characteristic parameters, such as counts, amplitude, energy, duration, and others [12]. Thus, the waveform of the AE signal can be described and compared with that of the vibration signal, as shown in Figures 2 and 3(a). Though the waveform of AE envelope signals is similar to that of vibration signals, the mechanisms are different. The rotor comes in contact with the stator once per revolution and the resulting shaft motion is a truncation of the synchronous response (Figure 2 is the assumed shaft motion and reference [2] also gives the experimental ones). The waveform also seems to be truncated in Figure 3, but, it is not because of the contact, it is because there is no rubbing between the rotor and the stator. The FFT plot of the AE signal is also similar to that of the vibration signal if rubbing occurs. But if the rubbing does not occur, there are usually no distinct harmonics, which will occur in the FFT plot of vibration signals.

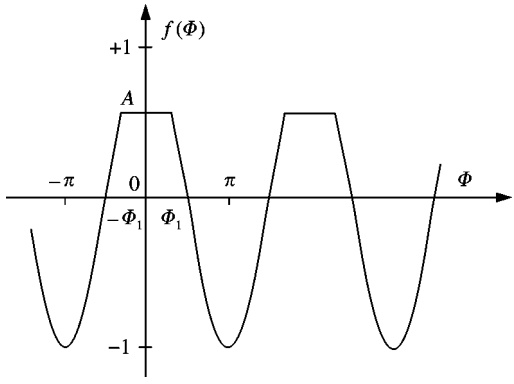

Figure 2. Assumed shaft motion.

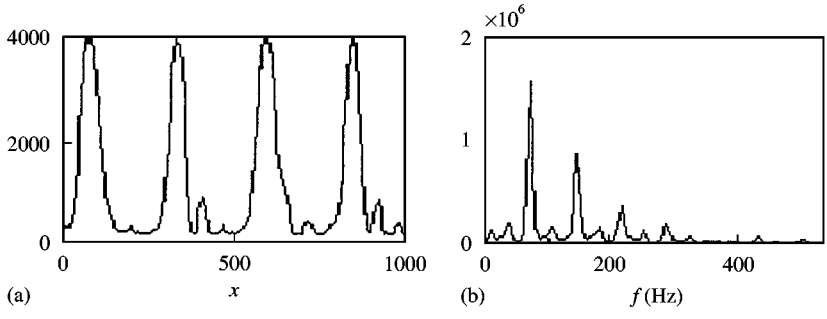

Figure 3. (a) AE signal, (b) FFT plot for AE signal.

4. DIRECT CROSS-CORRELATION METHOD

4.1. THE CROSS-CORRELATION METHOD

The cross-correlation is a conventional method for position pinpointing and AE sensors are usually used to locate the fault point. A common example is the location of the leakage area, as shown in Figure 4. With equation (1), the position can be calculated as

$$S = \frac{L - V\tau_0}{2}, \tag{1}$$

where S is the distance between the leakage point and sensor A, L is the distance between sensors A and B, V is the velocity of sound propagation in the structure, and τ_0 is the gap between the arrival times of the two sensors.

In equation (1), L can be measured directly. τ_0 is usually calculated with the cross-correlation function $R_{xy}(\tau)$, but to compare the sampled data separately, the normalized cross-correlation coefficient ρ_{xy} is used as in

$$\rho_{xy} = \frac{R_{xy}(\tau) - m_x m_y}{\sigma_x \sigma_y}, \tag{2}$$

where m_x and m_y are the mean values of the two signals respectively, σ_x and σ_y are the r.m.s. of the two signals respectively. When ρ_{xy} reaches its maximum value, the corresponding τ is τ_0.

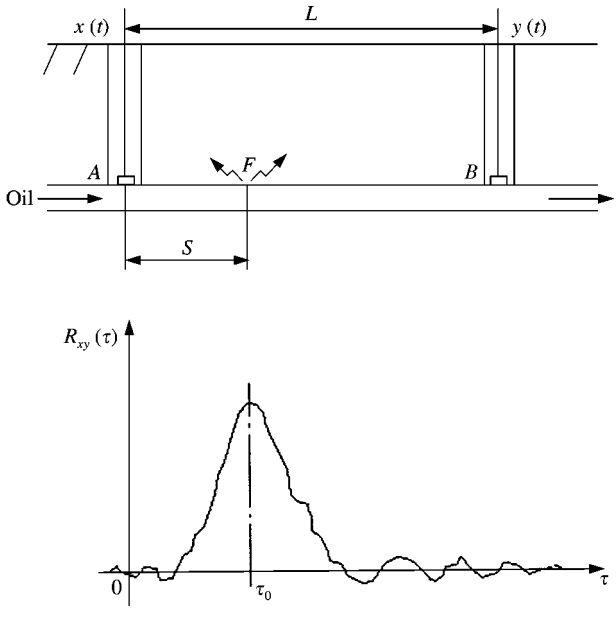

Figure 4. Locating of the leakage area.

Another important parameter is V. Sound can propagate as transversal wave, longitudinal wave or surface wave. Due to the situation of the placement of the sensors, the velocity for transversal wave in long rod is used [14]:

$$V = \sqrt{\pi r f}\ \sqrt[4]{\frac{E}{\rho}}, \tag{3}$$

where r is the radius of the axle, f is the frequency of sound (here the geometrical mean of the lowest and the highest frequencies of the band pass is used, 50 kHz), E is Young's modulus, and ρ is the density of steel. Finally, V can be obtained as 2224·2 m/s.

4.2. INSUFFICIENCY OF THE DIRECT CROSS-CORRELATION METHOD

Though the cross-correlation is very useful in position pinpointing for cases such as structural defects, when it is applied directly to the data of rubbing, it seems incapable. The insufficiency of the direct cross-correlation method (DC method) to the data of rubbing is tested by the following example.

The experiment was carried out using the rotor kit shown in Figure 1. The right rubbing screw was used to cause rubbing. The actual S was defined as the distance between the rubbing point and the middle of the fourth bearing housing, that is, 65·5 mm. Sensors A and B were on the third and fourth bearing housings respectively. The sampling frequency was 18181·8 Hz, and the length of each datum is $N = 2048$ points.

The sampled data are shown in Figure 5, with the form of the time-domain signals and FFT plots. Estimation of the normalized cross-correlation functions for the AE signals is shown in Figure 6. The cross-correlation sequence contains 4095 points (i.e., $2N - 1$ points) and the middle of the sequence represents the zeroth time lag between the signals from

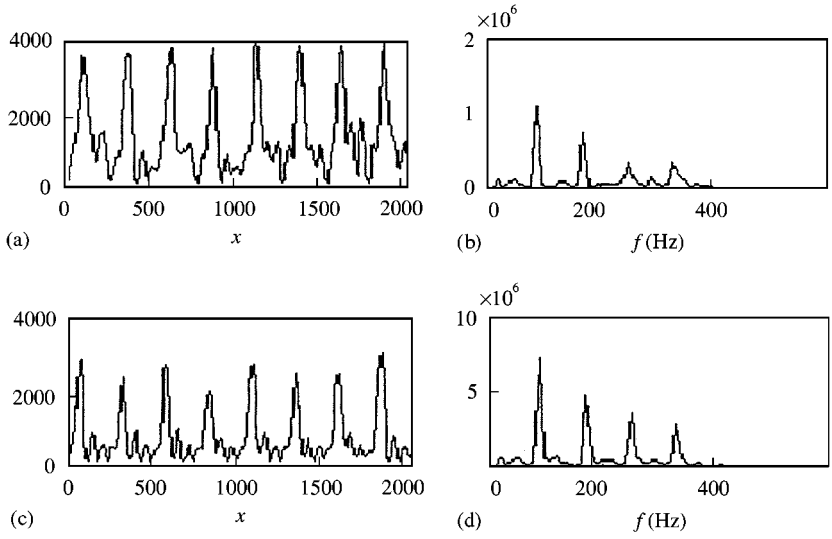

Figure 5. (a), (b) Signal and FFT of signal from sensor A; (c), (d) Signal and FFT of signal from sensor B.

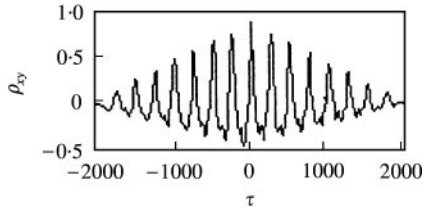

Figure 6. Cross-correlation of sensors A and B.

sensors A and B. The maximum correlation, ρ_{max}, is 0·8962 and the corresponding τ_0 is 0·0020. Then S can be calculated with equation (1) and gives the result as $S = -801$ mm. Obviously, this value does not agree with the actual S.

There may be four reasons for the discrepancy discussed above. Firstly, dynamic phenomena occur during rubbing, such as friction, impacting, stiffening and coupling effects, which makes the original signal more complicated. Secondly, the structural characteristics of the rotor system are rather complex, which may influence the propagation of sound. Actually, the form of the initial wave changes profoundly during propagation through the medium, and the signal emerging from the sensor has little resemblance to the original pulse [15]. Therefore, the path as well as the material is an important factor. Thirdly, the influence of oil film on the propagation of sound seems very little since the film is usually very thin. But whether there is sound produced in the film and what the influence is need more research. Fourthly, a big difference between rubbing and other types of fault such as cavitation is that rubbing will induce vibration in both the rotor and the stator simultaneously, and both parts, which will go through different paths, contribute to the energy received by AE sensors.

Due to various influences including the four reasons mentioned above, the method of direct cross-correlation could seldom produce the right answer. If some of the influences can be removed from the signals, maybe better results can be achieved. Suppose that from the viewpoint of frequency domain, there are some frequency bands where there are no or slight

noises, then the influences mentioned above could be removed to a great extent if the "uncontaminated" band of signal could be picked out. The wavelet transform is just such a useful tool to decompose the frequency domain, and thus makes it convenient to pick out the right band of signal.

5. WAVELET TRANSFORM CROSS-CORRELATION METHOD

5.1. WAVELET TRANSFORM

Wavelet theory was initially proposed by a geophysicist J. Morlet and a theoretical physicist A. Grossmann. Initially, wavelets were very much in the realm of pure mathematics and, as such, concentrated more on the theory than the application. The two America-based researchers Daubechies and Mallat changed this by defining the connection between wavelets and digital signal processing [16].

Wavelets have been applied to a number of areas, including data compression, image processing and time–frequency spectral estimation. This paper, however, concentrates upon the application of WT to decompose the signals.

Wavelet analysis provides a method for decomposing a signal into one of different possible families of orthogonal local basis functions called wavelets, as shown in the equation

$$f(x) = a_0\phi(x) + a_1\psi(x) + \cdots + a_{2^j+k}\psi(2^j x - k) + \cdots, \tag{4}$$

where

$$a_0 = \int_{-\infty}^{+\infty} f(x)\phi(x)\,\mathrm{d}x, \qquad a_{2^j+k} = 2^j \int_{-\infty}^{+\infty} f(x)\psi(2^j x - k)\,\mathrm{d}x, \tag{5}$$

with ϕ being the scaling function, and ψ the wavelet function. The coefficients $a_1, a_2, \ldots,$ represent the amplitudes of each of the contributing wavelets in a similar manner that the Fourier series coefficients are the amplitudes of the various sine and cosine terms in the classical Fourier analysis.

The discrete wavelet transform (DWT) is an algorithm for finding the coefficients in equation (6). Mallat's pyramid algorithm [17], as shown in Figure 7, solves for the coefficients without finding the scaling and wavelet functions directly and is very efficient computationally. The $h(n)$ or $g(n)$ in Figure 7 is quadrature mirror filter (QMF), and

$$c_k^j = \sum_n c_k^{j-1}\bar{h}_{n-2k}, \qquad d_k^j = \sum_n c_k^{j-1}\bar{g}_{n-2k} \quad (k = 0, 1, 2, \ldots, N-1). \tag{6}$$

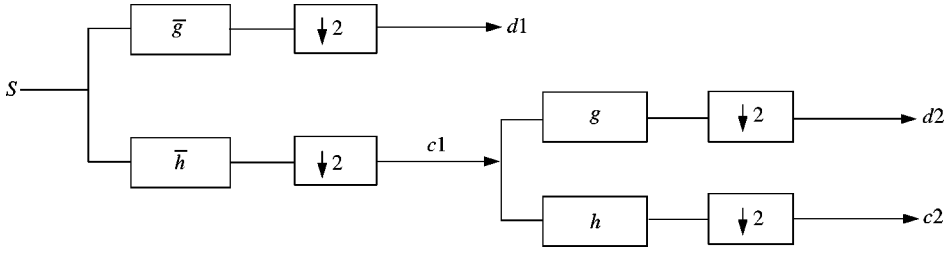

Figure 7. Discrete wavelet transform.

When a signal is decomposed into j levels with DWT, there are totally $j+1$ wavelet components at level j as a result, i.e., in the frequency domain, $0 \sim f_{max}$ is decomposed equally into

$$0 \sim \frac{1}{2^j} f_{max}, \frac{1}{2^j} f_{max} \sim \frac{1}{2^{j-1}} f_{max}, \cdots, \frac{1}{2} f_{max} \sim f_{max}.$$

If the width of the bands of higher frequency is not "slender" enough, the wavelet packet transform can be used. The difference between DWT and wavelet packet is that DWT decomposes only the approximation C_k^{j-1} while wavelet packet transform decomposes both the approximation and the detailed signal, as described in the equation

$$\mu_{2n}(x) = \sum h_k \mu_n(2x-k), \qquad \mu_{2n+1}(x) = \sum g_k \mu_n(2x-k), \tag{7}$$

where $\mu_0(x) = \phi(x)$ and $\mu_1(x) = \psi(x)$. Thus, when a signal is decomposed into j levels using wavelet packet, $0 \sim f_{max}$ is decomposed equally into

$$0 \sim \frac{1}{2^j} f_{max}, \frac{1}{2^j} f_{max} \sim \frac{2}{2^j} f_{max}, \cdots, \frac{2^j - 1}{2^j} f_{max} \sim f_{max},$$

totally 2^j wavelet components.

5.2. WAVELET TRANSFORM—CROSS-CORRELATION METHOD

The effect of the wavelet transform will be illustrated by the following example of the simulated signals. First, the signals are decomposed using wavelet packets, then the concerned bands are picked out and the cross-correlation method is used, and finally, the results are analyzed.

Signals x and y are defined as in equation (8), and their waveforms are illustrated in Figure 8. The sampling frequency is 2048 Hz. Obviously, the phase differences of the three

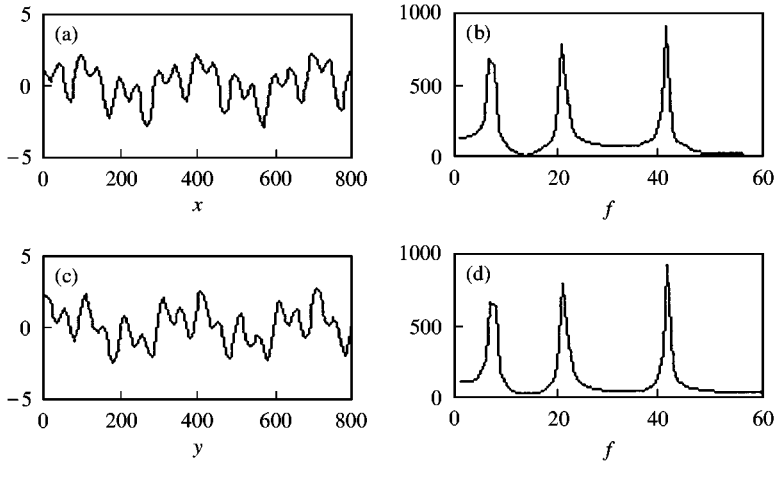

Figure 8. (a), (b) Signal x and its FFT plot; (c), (d) Signal y and its FFT plot.

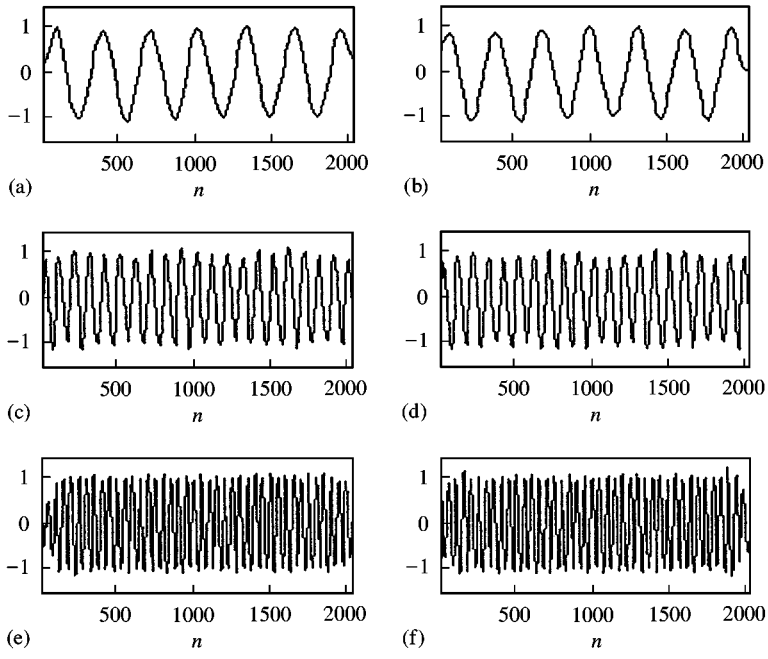

Figure 9. Wavelet transform of signals x and y.

sine waves are 20, 0, -10 respectively. The result of the DC method is $\rho_{max} = 0{\cdot}8925$ and $\tau_0 = -7$:

$$x = \sin\left(\frac{n}{50}\right) + \sin\left(\frac{n+10}{16}\right) + \sin\left(\frac{n+20}{8}\right),$$
$$y = \sin\left(\frac{n+20}{50}\right) + \sin\left(\frac{n+10}{16}\right) + \sin\left(\frac{n+10}{8}\right), \qquad n = 1, 2, 3, \ldots, 2048. \tag{8}$$

Three frequencies of the two signals can be calculated from equation (8). They are 6·5190, 20·3718 and 40·7437 Hz, as shown in Figures 8(b) and 8(d). The signals are decomposed into six levels with wavelet packet, i.e., the width of each frequency band is 16 Hz. Thus each frequency is in a separated band from other frequencies. The first three bands, which contain the frequencies of the two signals, are shown in Figure 9. Then the cross-correlation method can be used in Figures 9(a, b), 9(c, d) and 9(e, f) respectively. Three results are given as $\rho_{ab} = 0{\cdot}9970$, $\rho_{cd} = 0{\cdot}9956$, $\rho_{ef} = 0{\cdot}9903$, and τ_0 is 20, 0, -10 respectively.

Compared with the result of the DC method, the merit of decomposition can be seen: not only the two signals are more related for frequencies in these bands, but also the phase differences are accurate. Similarly, if this method is applied to the experimental data, a more accurate τ_0, and thus the position, can be expected. However, there are totally 2^j answers of τ_0 if the signals are decomposed into j levels using wavelet packets, and only one τ_0 should be right with the experimental data. The right τ_0 should be picked out from others. With the assumption that only the sound waves coming from the same source will be the most similar, the τ_0 can be picked out according to the maximum cross-correlation coefficient ρ_{max} and S can thus be calculated. The whole process can be called the wavelet transform cross-correlation (WTC) method.

TABLE 1

Positions of sensors and sources of sound†

Experiment No.	BH1	BH2	BH3	BH4	Distance between SS and sensors (mm)	
					*D*1	*D*2
1	S1, S2				113	113
2				S1, S2	767	767
3	S1			S2	113	767
4	S2			S1	767	113
5	S1, S2				87	87
6			S1	S2	65·5	311·5
7			S2	S1	311·5	65·5
8	S1			S2	87	793

†*Note*: BH is the bearing housing, S the sensor, SS the source of sound (rub point or excitation point), *D*1 the distance between SS and sensor 1, and *D*2 the distance between SS and sensor 2.

6. EXPERIMENTAL RESULT AND DISCUSSION

A series of experiments have been performed, while only eight of them are chosen to illustrate the power of the method proposed in this paper. In these experiments, the positions of the sensors were changed frequently from the side of one bearing housing to another, and sometimes both sensors were placed on the different sides of one bearing housing. In Table 1, the positions of sensors in the experiments are shown. These experiments were also carried out under different running conditions. Experiments 1–4 were done when the rotor was stationary, and experiments 5–8 were done when the rotor was running at the rated speed.

When the rotor was stationary, an excitation source, which could produce pulses of 40 Hz, was used to produce vibration. The force (smaller than 0·1 N) produced by the excitation source was in the axial direction and through the point on the left-most disc. In the experiments when the rotor was running, rub screws were used at different positions to produce rub. The positions of rub screws and the excitation point are also shown in Table 1 in terms of distances between them and sensors.

The band of the low-pass filter of the data acquisition system is set to $0 \sim 300$ Hz. The length of each datum is 2048. The wavelet used is db20 (Daubechies series with $N = 20$). The decomposition level is 8 and thus $0 \sim f_{max}$ (f_{max} is the sampling frequency) is decomposed equally into 256 bands. With the sampling frequency of 18181.8 Hz and the velocity of the sound calculated with equation (3), the resolution of location can be calculated as $\Delta S = 61{\cdot}2$ mm. This resolution is a little big, mainly due to the limit of the sampling frequency of the data acquisition system, but it is not a big problem for us to estimate the proposed method.

Experiments 1 and 2 were used to check if there was any inherent difference between the two sensors when they were mounted to measure the vibration of the rotor. Therefore, they were placed as close as possible, expecting to receive sound wave at the same point, but it could not be the real same point because there was always a small gap between the two sensors. Consequently, the sound waves received by the two sensors might still be quite different. This can explain why the cross-correlation coefficient ρ_{max}'s were not equal to 1·0, when the DC method was applied to the data of experiments 1 and 2, as shown in Table 2. It

TABLE 2

The results of DC and WTC methods in experiments 1, 2 *and* 5†

Experiment no.	DC method		WTC method		Actual ΔT (10^{-3} s)	Distance between SS and sensors (mm)
	ρ_{max}	ΔT (10^{-3} s)	ρ_{max}	ΔT (10^{-3} s)		
1	0·9811	0	0·9921	0	0	113
2	0·8901	6·7	0·9850	0	0	767
5	0·9118	6·7	0·9940	0	0	87

†*Note*: ΔT is the time difference between the two sensors in receiving the sound wave from the same source.

can also be seen from results of experiments 1 and 2 that the larger the distance between sensors and the source of sound, the smaller the ρ_{max}. This is reasonable because the form of the initial wave keeps changing during the propagation through the medium and a longer distance will cause more change. But when the rotor was running, some factors other than the distance seem to play a more important role in effecting the similarity of the sound waves received by the two sensors, as shown in experiment 5.

For experiment 1, it could be reasonable to assume that the excitation point is the only source of sound generated by the excitation force, since the force was too small to make the whole axle move and frictionize with the bearings to produce sound (notice that no oil film was present between the rotor and the bearing when the rotor was stationary). Different from the simple case in experiment 1, the situation in experiment 5 was more complex, as mentioned in section 4.2. Besides the rub, the noise could be generated from oil film, the motor or the rotor. The transmitting paths could be through rotor or the stator. Different paths can lead to a big difference in the transmitting of the sound. The speed of sound in the rotor is 2224·2 m/s, as calculated in section 4, while the speed of sound in the stator can be calculated as

$$\sqrt{\frac{E}{\rho}} = 5249 \text{ m/s},$$

where E and ρ are defined in the same way as in equation (3). Therefore, if sound waves transmit through both ways and merge eventually at the sensors, they will be much less similar to the original ones. So far, these influences could only be analyzed approximately, and more research work needs to be done.

The results of the other five experiments are shown in Table 3. Experiments 3 and 4 could be used to calibrate the speed of sound in the rotor. It can be seen that the S in experiments 3 and 4 are a little bigger than their true values. In equation (1), S and L are easy to measure with little error, τ_0 can be obtained with the sampled data, and V is calculated with equation (3). If the sampled data are fairly good (which means that τ_0 is measured with enough accuracy), there must be some error in the calculation of the velocity. Most probably, this error came from the frequency of the sound. The filter band of the sensor is 20 kHz $\sim$ 1·5 MHz and the frequency used in the calculation is 50 kHz. A slightly smaller frequency should be used in the calculation of the velocity.

Experiments 6 $\sim$ 8 were three examples that were used to locate the rubbing location. Apparently, the results of experiments 6 and 7 calculated with the DC method are too far from the actual values. The only difference between experiment 5, whose result is acceptable, and experiment 6 or 7 is the positions of the sensors. Therefore, different positions (thus different distances), combining different paths (thus different speeds) should be one of the

TABLE 3

The results of DC and WTC methods[†]

Experiment no.	DC method		WTC method		Actual
	ρ_{max}	S (mm)	ρ_{max}	S (mm)	S (mm)
3	0·7558	275	0·9116	214	113
4	0·7075	807	0·9082	807	767
6	0·9064	− 1708	0·9719	65·7	65·5
7	0·8962	− 555	0·9719	311·4	311·5
8	0·9087	162	0·9722	40	87

[†]*Note*: S is the distance between source of sound (rub point or excitation point) and sensor 1.

reasons. Another reason may be that when the rubbing screw was screwed down, rubbing may have occurred between the bearing and the shaft due to the pressure of the screw and thus there were multi-sources of rubbing. Although this kind of situation should have been avoided, it may have occurred.

Comparing the values of ρ_{max} with different methods, it is obvious that with the WTC method, the ρ_{max}'s are much closer to 1·0. It can also be seen that the signals are highly correlated for the relatively low frequencies (from experiments 1 to 8, the maximum correlated frequency bands are second, first, first, second, third, third, third, first in the total 256 bands). More importantly, S's are much closer to the real value. Therefore, the WTC method is useful in finding the more similar part of the signals and removing the influence of the noise and wave changes during propagation through the medium.

7. CONCLUDING REMARKS

Monitoring of rubbing and detection of the rubbing location with AE technique is a convenient and simple method. For instance, a higher accuracy of the location can be achieved by only using a higher sampling frequency. The rotor-to-stator rub will generally show very complicated dynamic characteristics. Owing to the influences of impacting, the structural characteristic, oil film, noise, system vibration and other factors, the conventional cross-correlation method does not give good result for detecting the rubbing location. Therefore, a wavelet transform cross-correlation method is proposed and experiments have shown that this method is effective in improving the accuracy of the results.

ACKNOWLEDGMENTS

This research is supported financially by a project from Ministry of Science and Technology in China (Grant No. PD9521908Z2) and Tsinghua University Basic Research Foundation (Grant No. Jc1999045).

Co-operation in the experiment and constructive discussions with Mr Li Huailing from Beijing Machinery Design Research Institute are highly appreciated.

REFERENCES

1. A. MUSZYNSKA 1989 *The Shock and Vibration Digest* **21**, 3–11. Rotor-to-stationary element rub-related vibration phenomena in rotating machinery literature survey.

2. R. F. BEATTY 1985 *Transactions of the American Society of Mechanical Engineers Journal of Vibration, Acoustics, Stress, and Reliability in Design* **107**, 151–160. Differentiating rotor response due to radial rubbing.
3. F. K. CHOY and J. PADOVAN 1987 *Journal of Sound and Vibration* **113**, 529–545. Non-linear transient analysis of rotor-casing rub events.
4. F. CHU and Z. ZHANG 1997 *International Journal of Engineering Science* **35**, 963–973. Periodic, quasi-periodic and chaotic vibrations of a rub-impact rotor system supported on oil film bearings.
5. A. F. ARMOR, L. J. GRAHAM and R. L. FRANK 1981 *American Society of Mechanical Engineers* (*Paper*). Oct 4–8, 12 pp. Acoustic emission monitoring of steam turbines.
6. Y. SHAO, A. ZHANG and R. YE 1999 *Modern Electric Power* **116**, 16–20. Monitoring friction between rotor and stationary of steam turbine by acoustic emission signal.
7. A. B. OKS, T. IWATSUBO and S. ARII 1993 *JSME International Journal Series C* **36**, 312–318. Detection of the point where rubbing occurs in a multisupported rotor system.
8. S. Y. LIANG and D. A. DORNFELD 1989 *Transactions of the American Society of Mechanical Engineers Journal of Engineering for Industry* **111**, 199–204. Tool wear detection using time series analysis of acoustic emission.
9. M. SURGEON and M. WEVERS 1999 *Materials Science and Engineering A*: *Structural Materials*: *Properties, Microstructure and Processing* **265**, 254–261. One sensor linear location of acoustic emission events using plate wave theories.
10. W. A. WILKINSON and M. D. COX 1996 *IEEE Transactions on Power Systems* **11**, 2038–2044. Discrete wavelet analysis of power system transients.
11. T. J. HOLROYD 1997 *Measurement and Control* **30**, 141–145. Acoustic emission—an NDT technique evolving into a versatile industrial monitoring method.
12. J. WU, J. LIANG and H. LI 1998 *Journal of Beijing University of Aeronautics and Astronautics* **24**, 104–107. Acoustic emission apparatus for rubbing diagnosis of large rotating machinery.
13. S. J. VAHAVIOLOS, A. POLLOCK and N. LEW 1991 *Chemical Engineering Progress* **87**, 60–66. Pinpoint structural defects with acoustic emissions.
14. R. WANG 1983 *Handbook of Underwater Sound Materials*. Beijing: Science Press.
15. A. A POLLOCK 1986 *The Japanese Society for Nondestructive Inspection* 708–721. Classical wave theory in practical AE testing.
16. P. M. BENTLEY and J. T. E. MCDONNELL 1994 *Electronics and Communication Engineering Journal* **6**, 175–186. Wavelet transforms: an introduction.
17. S. MALLAT 1989 *IEEE Transactions on Pattern Analysis and Machine Intelligence* **11**, 674–693. A theory for multiresolution signal decomposition: the wavelet representation.